Numerical modeling of algebraic closure models of oceanic turbulent mixing layers

A. C. Bennis*, T. Chacón Rebollo †, M. Gómez Mármol ‡, R. Lewandowski §

Abstract

We introduce in this paper some elements for the mathematical and numerical analysis of algebraic turbulence models for oceanic surface mixing layers. In these models the turbulent diffusions are parameterized by means of the Richardson's number, that measures the balance between stabilizing buoyancy forces and un-stabilizing shearing forces. We prove the stability of conservative finite difference approximations. We analyze the existence and stability of equilibria state, and introduce a new scheme that has only one equilibrium state. We also analyze the well-possedness of a simplified model. We finally present some numerical tests for realistic flows in tropical seas that reproduce the formation of mixing layers, in agreement with the physics of the problem.

Keywords: Turbulent mixing layers, Richardson's number, First order closure models, Conservative numerical solution, Stability of steady states, Tests for tropical seas
AMS classification: 76D05, 35Q30, 76F65, 76D03

1 Introduction

This paper is devoted to the mathematical and numerical analysis of turbulence models of surface oceanic mixing layers. In a context of global climate change, the accurate simulation of the Surface Sea Temperature (SST) is of primary importance, as it affects the global oceanic circulation, and has a deep impact in the evolution of polar ices (Cf. Goose et al. [4]). This problem is being analyzed by the physical oceanography community since the early 80's. One of their main objectives is to build mathematical models to achieve a right numerical simulation of SST, mainly in Tropical Ocean areas, as these areas receive large amounts of solar heat that is brought into the oceanic global energy balance.

The parametrization of turbulence in the mixing layer must take into account the two forces that act in the momentum and mass exchange produced by mixing effects: Buoyancy and shear. The

*IRMAR, Université de Rennes 1, Campus de Beaulieu, 35042 Rennes Cedex, France

†Departamento de Ecuaciones Diferenciales y Análisis Numerico, Universidad de Sevilla. C/Tarfia, s/n. 41080, Sevilla, Spain

‡Departamento de Ecuaciones Diferenciales y Análisis Numerico, Universidad de Sevilla. C/Tarfia, s/n. 41080, Sevilla, Spain

§IRMAR, Université de Rennes 1, Campus de Beaulieu, 35042 Rennes Cedex, France

early class of models parameterize the turbulent viscous and diffusion in terms of the Richardson number by means of algebraic expressions. The Richardson number measures the rate between stabilizing buoyancy forces and un-stabilizing shearing forces. One of the most popular of these models was introduced by Pacanowski and Philander in 1981 [11]. This description in terms of the Richardson number allows large mixing in zones of low stratification, and inhibits it in zones of strong stratification. This model was modified in several ways, in order to obtain a better fitting with experimental measurements. One of these improvements was proposed by Gent in 1991 (Cf. [3]). Another kind of improvements was based upon the parametrization of the vertical profile of turbulent kinetic energy (KPP model, Cf. Large and Gent, [6]). All these are vertical 1D models based upon the knowledge of the atmospheric forcing to set the boundary conditions. More classical turbulence models of k-ε kind, have also been developed, taking into account buoyancy effects. Let us mention for instance the second order closure models of Mellor and Yamada [10] and Gaspar et al. [2].

In the recent years, the mathematical community has shown an increasing interest in the theoretical and numerical analysis of geophysical flow problems. This interest has been mainly addressed to models for large-scale atmospheric and oceanic flows, frequently using shallow water approaches. In the case of water flows, rather little attention has been addressed to buoyant turbulence effects. However, the behavior of SST deeply depends on a correct description of the turbulent mass and momentum mixing in the upper oceanic layer, where buoyancy plays a key role.

Our purpose in this paper is to give some mathematical and numerical insight to the analysis of the algebraic Richardson number-based models mentioned above. Our main contribution is to show that the usual conservative numerical schemes used by the physical oceanography community to solve them are well suited, in the sense that they are stable and verify a maximum principle. We also perform an analysis of existence of equilibrium solutions and prove their stability, in order to analyze their long-time behavior, which is relevant for the long-term calculations of SST. In this context, we introduce a new model which just has one equilibrium state, avoiding the non-physical multiplicity of the standard models.

We also give an existence result for a simplified model based upon a compactness argument, although not for the general models we are dealing with. The analysis of well-possedness of Richardson number-based models is a difficult mathematical problem mainly due to the the lack of monotonicity. This avoids to obtain estimates in a sense strong enough to deal with the nonlinear turbulent diffusions. The key difficulty is that these diffusions depend on the gradients of temperature and velocity, but we only may prove the standard estimates for parabolic equations. Our simplified result is based upon a description of the temperature equation using its vertical gradient as unknown. This equation is genuinely parabolic for some particular configurations of the turbulent diffusion.

The paper is organized as follows: In section 2 we describe the Richardson-based models we are interested in, and their physical motivation. Section 3 is devoted to the analysis of the simplified model mentioned below. We next analyze the existence of equilibria states, proving that these

necessarily correspond to linear profiles of velocity and temperature (or salinity), and introduce a new model that has just one equilibrium state (Section 4). We also analyze the stability of these equilibria, and prove that at least one is stable for vertical stable configurations (Section 5). We next prove the stability of the usual conservative numerical schemes used to solve these models, and prove a maximum principle (Section 6). We present some numerical tests for realistic flows in tropical seas that reproduce the formation of mixing layers, in agreement with the physics of the problem. We stress that our new model produces results very close to the PP one, and in addition is able to handle statically unstable initial data (Section 7). Finally, we address some conclusions (Section 8).

2 Setting of model problems

The wind-stress generates intense mixing processes in a layer below the ocean surface. This layer has two parts, the upper one is an homogeneous layer, known as the mixed layer. This layer presents almost-constant temperature (and salinity). The bottom of the mixed layer corresponds to the top of the pycnocline, a thin layer with a large gradient of density. For instance, in tropical seas a sharp thermocline is formed. In this last layer still mixing processes do occur, but it has not a homogeneous structure. The zone formed by the two layers is known as the mixing layer. Its thickness may vary between ten meters and a few hundred of meters, depending on the latitude. It also presents seasonal variations.

Typically, the variables used to describe the mixing layer are the statistical means of horizontal velocity (u, v) and density ρ. In the ocean, the density is a function of temperature and the salinity through a state equation. So, we consider the density as an idealized thermodynamic variable which is intended to represent temperature and salinity variations. We are mainly interested in tropical seas, where the salinity in the mixing layer is almost constant, and the density is just a function of the temperature.

The mixed layer being strongly dominated by vertical fluxes, velocity, density and pressure are supposed to be horizontally homogeneous. We assume

$$U = (u(z,t), v(z,t), w(z,t)), \quad \rho = \rho(z,t), \quad p = p(z,t).$$

This leads to one-dimensional models depending only on the vertical variable. The Coriolis force is neglected, a good approximation in tropical oceans. Therefore, the equations governing the mixing layer, obtained by statistical averaging of Navier-Stokes equations, are

$$\begin{cases} \dfrac{\partial u}{\partial t} - \alpha_1 \dfrac{\partial^2 u}{\partial z^2} = -\dfrac{\partial}{\partial z} \langle u'\, w' \rangle , \\ \dfrac{\partial v}{\partial t} - \alpha_1 \dfrac{\partial^2 u}{\partial z^2} = -\dfrac{\partial}{\partial z} \langle v'\, w' \rangle , \\ \dfrac{\partial \rho}{\partial t} - \alpha_2 \dfrac{\partial^2 \rho}{\partial z^2} = -\dfrac{\partial}{\partial z} \langle \rho'\, w' \rangle , \end{cases} \tag{1}$$

where $(u', v'), w', \rho'$ represent the fluctuations of the horizontal velocity, vertical velocity and density, and α_1, α_2 are the laminar viscosity and diffusion. The notation $\langle \ \ \rangle$ signifies that the

quantity is statistically averaged, in the usual sense used in turbulence modeling. Equations (1) are the classical equations corresponding to a modeling of a water column. Equations (1) are not closed. To close them, the vertical fluxes appearing in the right-hand side need to be modeled. The Richardson number-based models use the concept of eddy diffusion in order to represent turbulent fluxes. So we set

$$-\left\langle u'\,w'\right\rangle = \nu_{T1}\frac{\partial u}{\partial z}, \quad -\left\langle v'\,w'\right\rangle = \nu_{T1}\frac{\partial v}{\partial z}, \quad -\left\langle \rho'\,w'\right\rangle = \nu_{T2}\frac{\partial \rho}{\partial z}.$$

ν_{T1} and ν_{T2} are the vertical eddy viscosity and diffusivity coefficients, which are expressed as functions of the gradient Richardson number R defined as

$$R = -\frac{g}{\rho_0}\,\frac{\dfrac{\partial \rho}{\partial z}}{\left(\dfrac{\partial u}{\partial z}\right)^2 + \left(\dfrac{\partial v}{\partial z}\right)^2},$$

where g is the gravitational acceleration and ρ_0 a reference density (for example $\rho_0 = 1025\, kg.m^{-3}$). The gradient Richardson number is the ratio between the stabilizing vertical forces due to buoyancy and the un-stabilizing horizontal ones due to shear in a water column.
When $R >> 1$, a strongly stratified layer takes place. This correspond to a stable configuration. When $0 < R << 1$, a slightly stratified layer takes place. This correspond to a configuration with low stability. The case $R < 0$ corresponds to a configuration statically unstable ($\dfrac{\partial \rho}{\partial z} > 0$), that in fact we are not modeling. However, we must handle this situation for our numerical experiments. A simple way is to set large constant values for the turbulent diffusions in this case, althoug we shall need a smoother modeling for our analysis.
The set of equations, initial and boundary conditions governing the mixing layer can now be written

$$\begin{cases} \dfrac{\partial u}{\partial t} - \dfrac{\partial}{\partial z}\left(\nu_1 \dfrac{\partial u}{\partial z}\right) = 0, \\ \dfrac{\partial v}{\partial t} - \dfrac{\partial}{\partial z}\left(\nu_1 \dfrac{\partial v}{\partial z}\right) = 0, \\ \dfrac{\partial \rho}{\partial t} - \dfrac{\partial}{\partial z}\left(\nu_2 \dfrac{\partial \rho}{\partial z}\right) = 0, \text{ for } t \geqslant 0 \text{ and } -h \leqslant z \leqslant 0, \\ u = u_b,\ v = v_b,\ \rho = \rho_b \text{ at the depth } z = -h, \\ \nu_1 \dfrac{\partial u}{\partial z} = \dfrac{\rho_a}{\rho_0} V_x,\ \nu_1 \dfrac{\partial v}{\partial z} = \dfrac{\rho_a}{\rho_0} V_y,\ \nu_2 \dfrac{\partial \rho}{\partial z} = Q \text{ at the surface } z = 0, \\ u = u_0,\ v = v_0,\ \rho = \rho_0 \text{ at initial time } t = 0. \end{cases} \tag{2}$$

In system (2), $\nu_1 = \alpha_1 + \nu_{T1}$, $\nu_2 = \alpha_2 + \nu_{T2}$ respectively are the total viscosity and diffusion. The constant h denotes the thickness of the studied layer that must contain the mixing layer. Therefore the circulation for $z < -h$, under the boundary layer, is supposed to be known, either by observations or by a deep circulation numerical model. This justifies the choice of Dirichlet

boundary conditions at $z = -h$, $(u_b,\ v_b)$ and ρ_b being the values of horizontal velocity and density in the layer located below the mixed layer. The forcing by the atmosphere is modeled by the fluxes at the sea-surface: V_x and V_y are respectively the stress exerced by the zonal wind-stress and the meridional wind-stress and Q represents the thermodynamical fluxes, heating or cooling, precipitations or evaporation. We have $(V_x, V_y) = C_D \left|U^a\right| U^a$, where $U^a = (u_a, v_a)$ is the air velocity and $C_D\,(= 1, 2.10^{-3})$ is a friction coefficient.
We study hereafter the modeling of the eddy coefficients made by the Pacanowski-Philander (PP) (Cf. [11]) and Gent (Cf. [3]) models. We write $\nu_1 = f_1(R)$ and $\nu_2 = f_2(R)$. In PP model, the functions f_1 and f_2 can be defined as

$$f_1(R) = \alpha_1 + \frac{\beta_1}{(1+5R)^2}, \quad f_2(R) = \alpha_2 + \frac{f_1(R)}{1+5R} = \alpha_2 + \frac{\alpha_1}{1+5R} + \frac{\beta_1}{(1+5R)^3}. \tag{3}$$

This formulation has been used in the OPA code developed by Paris 6 University by Delecluse and co-workers (Cf. [1], [8]) with coefficients

$$\alpha_1 = 1.10^{-6},\ \beta_1 = 1.10^{-2},\ \alpha_2 = 1.10^{-7}\left(\text{units: } m^2 s^{-1}\right).$$

The selection criterion for the coefficients appearing in these formulas was the best agreement of numerical results with observations carried out in different tropical areas.
A variant of formulation (3), proposed by Gent [3], is

$$f_1(R) = \alpha_1 + \frac{\beta_1}{(1+10R)^2}, \quad f_2(R) = \alpha_2 + \frac{\beta_2}{(1+10R)^3} \tag{4}$$

with $\alpha_1 = 1.10^{-4}$, $\beta_1 = 1.10^{-1}$, $\alpha_2 = 1.10^{-5}$, $\beta_2 = 1.10^{-1}$(units: $m^2 s^{-1}$). A formulation similar to (4) when replacing $10R$ by $5R$ and varying the values of the coefficients α_1, α_2 between the surface and the depth 50m is used in Goose et al. [4].
These models apply to vertically stable configurations, for which $\partial_z \rho \leq 0$, and then $R \geq 0$. Turbulence may be generated by the shear induced by the wind and by buoyancy forces, but the model describes the state of the flow once the vertical configuration has been stabilized by buoyancy forces. However, as we have already mentioned, for numerical simulations the case $R \leq 0$, that corresponds to unstable buoyant configurations, must be taken into account.

3 Analysis of a simplified model

The analysis of the well-possedness of problem (2) faces hard difficulties. This mainly occurs because on one hand the turbulent diffusions depend on the derivatives of the unknowns, and on another hand the space operator appearing in this equation could not to be monotonic in general. To illustrate this fact, we present the analysis of a simplified model for one equation, that may be viewed as the equation satisfied by the unknown ρ in system (2) once the velocity

field is known. This model reads

$$\partial_t \rho - \partial_z (f(\partial_z \rho)\partial_z \rho) = 0, \tag{5}$$

$$f(\partial_z \rho)\partial_z \rho|_{z=0} = Q_s, f(\partial_z \rho)\partial_z \rho|_{z=-h} = Q_b, \tag{6}$$

$$\rho(0) = \rho_0. \tag{7}$$

where for brevity we denote for any function $a = a(t, z)$, $\partial_z a = \dfrac{\partial a}{\partial z}$, $\quad \partial_t a = \dfrac{\partial a}{\partial t}$.
Here, $f(\theta)$ stands for the turbulent diffusion. We assume that this is a real function given by

$$f(\theta) = \alpha + \frac{\beta}{(1 - \gamma\,\theta)^m}, \quad \text{for some } \alpha > 0,\, \beta > 0,\, \gamma > 0,\, m > 0, \quad \text{for } \theta < 0. \tag{8}$$

This is a function with the same structure of the turbulent diffusions appearing in PP and Gent models, if we replace the Richardson number R by $\theta = -\partial_z \rho$. Negative values of θ correspond to stable vertical configurations. For positive θ, that correspond to unstable configurations, we may assume that f is increasing: For larger θ the water column is more unstable, and then the turbulent diffusion must also be larger.
We are interested in finding an equation for $\theta = \partial_z \rho$. This equation is formally obtained by deriving (11) with respect to z:

$$\partial_t \theta - \partial_z \left[\big(f(\theta) + f'(\theta)\,\theta \big)\, \partial_z \theta \right] = 0 \tag{9}$$

This appears as a non-linear parabolic equation with diffusion

$$g(\theta) = f(\theta) + f'(\theta)\,\theta.$$

When $0 < m \leq 1$, g is an increasing function, and $g(\theta) \geq \alpha$, $\forall \theta \leq 0$. However, for $m > 1$, g is negative in a range of negative θ. Indeed, g attains its minimum at $\theta_m = -\dfrac{2}{(m-1)\,\gamma}$ with value

$$g(\theta_m) = \alpha - \beta \left(\frac{m-1}{m+1} \right)^{m+1}.$$

For the physical values of α and β appearing in PP and Gent models, this value is negative. Thus, in general equation (9) is not well posed.
We may, however, prove an existence result for the cases in which g is uniformly positive:

$$\text{Either} \quad 0 < m < 1, \quad \text{or} \quad \alpha > \beta \left(\frac{m-1}{m+1} \right)^{m+1}. \tag{10}$$

Indeed, let us consider the problem

$$\partial_t \theta - \partial_z \left[\big(f(\theta) + f'(\theta)\,\theta \big)\, \partial_z \theta \right] = 0, \tag{11}$$

$$\theta|_{z=0} = \theta_s, \theta|_{z=-h} = \theta_b, \tag{12}$$

$$\theta(0) = \theta_0 = \partial_z \rho_0; \tag{13}$$

Here we set Dirichlet boundary conditions for θ deduced from the Newmann boundary conditions (6). We assume that the equation $f(\theta)\,\theta = Q_s$ admits a solution $\theta = \theta_s$, that we set as Dirichlet boundary condition at $z = 0$. And similarly at $z = -h$. We assume that

$$(H) \qquad f \in C^1(\mathbb{R}), \quad \nu \leq f(\theta) + f'(\theta)\,\theta \leq M, \tag{14}$$

for some $0 < \nu < M$. We assume that f is extended for positive values of θ satisfying the same conditions, but we do not give any explicit definition for these values. We may state the

Theorem 3.1 *Assume that Hypothesis (14) holds. Assume also that $\theta_0 \in L^2(-h,0)$, θ_s, $\theta_b \in H^1(0,T)$. Then problem (11)-(12)-(13) admits a weak solution in $L^2((0,T),H^1(-h,0)) \cap L^\infty((0,T),L^2(-h,0))$, with $\partial_t\theta \in L^2((0,T),[H^1(-h,0)]')$. This solution verifies the estimate*

$$\begin{aligned} \|\theta\|_{L^2((0,T),H^1(-h,0))} &+ \|\theta\|_{L^\infty((0,T),L^2(-h,0))} + \|\partial_t\theta\|_{L^2((0,T),[H^1(-h,0)]')} \leq \\ &\leq C\,\left[\|\theta_0\|_{L^2(-h,0)} + \|\theta_s\|_{H^1(0,T)} + \|\theta_b\|_{H^1(0,T)}\right]; \end{aligned} \tag{15}$$

where C is a constant depending on f, ν and h.

Proof. We use a compactness argument. Consider the Banach space

$$W = \{\theta \in L^2((0,T),H_0^1(-h,0)) \cap L^\infty((0,T),L^2(-h,0)),\ \text{s. t. } \partial_t\theta \in L^2((0,T),H^{-1}(-h,0))\}.$$

Given $\theta^{(n)} \in W$, consider the linear problem

$$\partial_t\theta^{(n+1)} - \partial_z\left[g(\theta^{(n)})\partial_z\theta^{(n+1)}\right] = 0, \tag{16}$$

$$\theta^{(n+1)}|_{z=0} = \theta_s, \theta^{(n+1)}|_{z=-h} = \theta_b, \tag{17}$$

$$\theta(0) = \theta_0; \tag{18}$$

Define $\sigma_0(z,t) = \dfrac{z+h}{h}\,\theta_s(t) + \dfrac{z}{h}\,\theta_b(t)$, and look for $\theta^{(n+1)} = \sigma^{(n+1)} + \sigma_0$. This problem admits the following variational formulation: Obtain $\sigma^{(n+1)} \in W$ such that $\forall v \in H_0^1(-h,0)$

$$\begin{aligned} \frac{d}{dt}\int_{-h}^0 \sigma^{(n+1)}\,v &+ \int_{-h}^0 g(\sigma^{(n)}+\sigma_0)\,\partial_z(\sigma^{(n+1)})\,\partial_z v = -\int_{-h}^0 \partial_t\sigma_0\,v \\ &+ \int_{-h}^0 g(\sigma^{(n)}+\sigma_0)\,\partial_z(\sigma_0)\,\partial_z v \quad \text{in } \mathcal{D}'(0,T), \end{aligned} \tag{19}$$

$$\sigma^{(n+1)}(0) = \sigma_0 = \theta_0 - \sigma(0) \quad \text{in } L^2(-h,0). \tag{20}$$

Note that $\partial_t\sigma_0 \in L^2((0,T),L^2(-h,0))$, and

$$\|\partial_t\sigma_0\|_{L^2((0,T),L^2(-h,0))} \leq \frac{2}{3}\,h\,\left[\|\theta_s\|^2_{H^1(0,T)} + \|\theta_b\|^2_{H^1(0,T)}\right].$$

Also, denote $L_{\sigma^{(n)}}(v) = \displaystyle\int_{-h}^0 g(\sigma^{(n)}+\sigma_0)\,\partial_z(\sigma_0)\,\partial_z v$. As

$$|L_{\sigma^{(n)}}(v)| \leq \frac{M}{h}\,\left[|\theta_s(t)| + |\theta_b(t)|\right]\,\|\partial_z v\|_{L^1(-h,0)},\ \text{a. e. } in (0,T)$$

we deduce that

$$\|L_{\sigma^{(n)}}(v)\|_{L^2((0,T),H^{-1}(-h,0))} \leq C_1 \left[\|\theta_s\|_{L^2(0,T)} + \|\theta_b\|_{L^2(0,T)}\right],$$

where the constant C_1 depends on M and h.
Then, due to hypothesis (14), by standard arguments, problem (19)-(20) admits a unique solution that satisfies the estimate

$$\|\sigma^{(n+1)}\|_W \leq C \left[\|\sigma_0\|_{L^2(-h,0)} + \|\theta_s\|_{H^1(0,T)} + \|\theta_b\|_{H^1(0,T)}\right], \tag{21}$$

where C depends on M, h and ν.
We now define a sequence $\{\sigma^{(n+1)}\}_{n\geq 1}$, starting from some $\sigma^{(0)} \in W$. Then, each $\sigma^{(n)}$ satisfies estimate (21), and we may extract a subsequence (that we denote in the same way) weakly convergent in W to some σ.
Applying Aubin-Lions Lemma, one deduces that $\{\sigma^{(n+1)}\}_{n\geq 1}$ is compact in $L^2((0,T)\times(-h,0))$ and hence (up to a subsequence) strongly converges to σ in $L^2((0,T)\times(-h,0))$ and thus (again up to a subsequence) almost everywhere in $Q_T = (-h,0)\times(0,T)$.
Define $\theta = \sigma + \sigma_0$. Then, $\lim_{n\to\infty} |g(\sigma^{(n)} + \sigma) - g(\theta)|^r = 0$ a. e. in Q_T, for any $r > 0$. Also, using hypothesis (14), $|g(\sigma^{(n)} + \sigma) - g(\theta)|^r \leq 2\,M$. We deduce from the Dominated Convergence Theorem that

$$\lim_{n\to\infty} g(\sigma^{(n)} + \sigma) = g(\theta) \quad \text{in} \quad L^r(Q_T),\ 1 \leq r < +\infty.$$

Consider now $v \in \mathcal{D}(-h,0)$, $\varphi \in \mathcal{D}(0,T)$. Then,

$$\lim_{n\to\infty} \int_0^T \int_{-h}^0 g(\sigma^{(n)} + \sigma_0)\, \partial_z(\sigma^{(n+1)})\, \partial_z v\, \varphi\, dz\, dt = \int_0^T \int_{-h}^0 g(\theta)\, \partial_z\sigma\, \partial_z v\, \varphi\, dz\, dt.$$

Similarly,

$$\lim_{n\to\infty} L_{\sigma^{(n)}}(v) = L_\sigma(v).$$

The remaining terms in (19) pass to the limit in a standard way. Then, we conclude that $\theta \in L^2((0,T),H^1(-h,0)) \cap L^\infty((0,T),L^2(-h,0))$ is a weak solution of problem (11)-(12)-(13) such that $\partial_t\theta \in L^2((0,T),[H^1(-h,0)]')$, and that satisfies estimate (15). •
Note that this results follows from the monotonicity of the elliptic operator appearing in problem (19), ensured by conditions (14) on f. This monotonicity is found when the space $L^2(0,T;L^2(-h,0))$ is used as pivot space. However, a different pivot space could be used, following Lions [7], chapter 2. This would yield the monotonicity under different conditions on f. This could be a way to prove the monotonicity of Richardson number-based models in more general situations.

4 Equilibria states

Although we are not able to analyze the model system (1) in general, it is possible to deduce its equilibria states and analyze their stability. This is, to analyze the asymptotic behavior of

the mixing layer for very long time periods. We shall prove that all equilibria states are linear profiles, with asymptotic stability as $t \to +\infty$.
The steady solutions satisfy the system

$$\begin{cases} \dfrac{\partial}{\partial z}\left(f_1(R)\dfrac{\partial u}{\partial z}\right) = 0, \\ \dfrac{\partial}{\partial z}\left(f_1(R)\dfrac{\partial v}{\partial z}\right) = 0, \\ \dfrac{\partial}{\partial z}\left(f_2(R)\dfrac{\partial \rho}{\partial z}\right) = 0. \end{cases} \tag{22}$$

Integration with respect to z yields:

$$\begin{cases} f_1(R)\dfrac{\partial u}{\partial z} = \dfrac{V_x \rho_a}{\rho_0}, \\ f_1(R)\dfrac{\partial u}{\partial z} = \dfrac{V_y \rho_a}{\rho_0}, \\ f_2(R)\dfrac{\partial \rho}{\partial z} = Q. \end{cases} \tag{23}$$

As $R = \dfrac{-\dfrac{g}{\rho_0}\cdot\dfrac{\partial \rho}{\partial z}}{\left(\dfrac{\partial u}{\partial z}\right)^2 + \left(\dfrac{\partial v}{\partial z}\right)^2}$, we deduce an implicit equation for R,

$$R = -g\,\frac{\rho_0}{\rho_a^2}\,\frac{Q}{V_x^2+V_y^2}\,\frac{f_2(R)}{(f_1(R))^2}. \tag{24}$$

If this equation has a solution, R^e, we obtain an equilibrium solution corresponding to the fluxes Q, V_x and V_y. More precisely, this solution depends on the fluxes ratio $r = \dfrac{Q}{V_x^2+V_y^2}$. It admits a meaningful physical interpretation: At equilibrium the ratio between potential and turbulent kinetic energy is proportional to the surface fluxes ratio,

$$\frac{\text{Potential energy}}{\text{Turbulent kinetic energy}}(\text{Equilibrium}) = \ \text{Constant}(R^e)\ \times \frac{Q}{V_x^2+V_y^2}.$$

As R^e, f_1 and f_2 are independent of z, we deduce the equilibrium profiles by integration in z of equations (23). These are

$$u^e(z) = u_b + \frac{V_x \rho_a}{\rho_0 f_1(R^e)}\,(z+h), \tag{25}$$

$$v^e(z) = v_b + \frac{V_y \rho_a}{\rho_0 f_1(R^e)}\,(z+h), \tag{26}$$

$$\rho^e(z) = \rho_b + \frac{Q}{f_2(R^e)}\,(z+h); \tag{27}$$

where we have included the Dirichlet boundary conditions at $z = -h$.

We next analyze the existence of solutions of equation (24). These solutions may be interpreted as the intersection of the curves

$$k\left(R\right)=\frac{\left(f_1\left(R\right)\right)^2}{f_2\left(R\right)}\quad\text{and}\quad h\left(R\right)=CR,\quad\text{with}\quad C=-\frac{\rho_a^2(V_x^2+V_y^2)}{gQ\rho_0}.$$

For each actual model, the existence and the number of solutions only depends on the value of the constant C (or, more specifically, on the fluxes ratio r).

PP and Gent models present the same qualitative behavior. We recall that these models are no more valid respectively for $R\leq R^*$ with $R^*=-1/5$ and $R^*=-1/10$ since the diffusion f_2 at these ranges is negative. For each one of these models, $k(R)$ is a strictly decreasing function for $R\geq 0$. This yields a unique equilibrium state for each model when the fluxes ratio $r\leq 0$ (which corresponds to statically stable configurations, $R>0$).

There is also a range $r^*>r>0$, for which equation (24) admits several solutions.

From a mathematical point of view this is coherent with the use of a different parametrization of eddy diffusions for $R<0$. Following this purpose to avoid the multiplicity of steady states, we introduce in this paper a new model, which is a slight modification of PP model. This new model is given by

$$f_1\left(R\right)=\alpha_1+\frac{\beta_1}{\left(1+5R\right)^2},\quad f_2\left(R\right)=\alpha_2+\frac{f_1(R)}{\left(1+5R\right)^2},\tag{28}$$

with the same constants as the PP model. This new model has a unique equilibrium R^e for any fluxes ratio r. As we shall see in the numerical tests, this model gives solutions very close to these provided by the PP model.

In the sequel we shall use the abridged notation Rijk to define each one of the three models we are considering. The indices i, j and k represent the exponents of the denominators in the definition of the turbulent diffusions f_1 and f_2. Thus, R213, R224 and R23 will respectively denote the PP, Gent and new models.

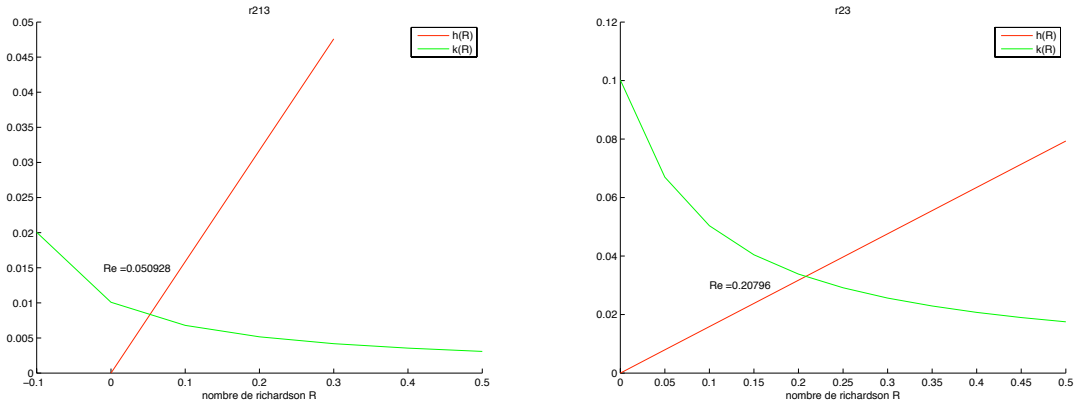

Figure 1:
Solution of the equation for equilibrium Richardson numbers for PP (left) and Gent models (right).

As an example, we present the equilibria Richardson numbers corresponding to realistic values (see section 7.1) We have taken $V_x = 35.10^{-3}\, m^2 s^{-2}$, $V_y = 97.10^{-5}\, m^2 s^{-2}$, and also a negative Q, $Q = -1.10^{-6}\, Kg.m^{-2} s^{-1}$, so we are in a situation of static stability.
We observe on figures 1 and 2 the only equilibrium solution corresponding to each model. From figure 2 it is clear that there exists a unique equilibrium solution for the new model, for any value of the fluxes ratio r.

5 Linear stability of equilibrium solutions

In this section, we analyze the stability of the equilibrium solutions. We prove that for all the three models considered, these equilibria are linearly stable for negative fluxes ratio r. This supports the well-possedness of all these models, at least for physically meaning equilibrium solutions.
Let us consider an initial perturbation of the form

$$(u_0, v_0, \rho_0) = (u^e, v^e, \rho^e) + \left(u_0', v_0', \rho_0'\right),$$

where (u^e, v^e, ρ^e) is an equilibrium solution, and (u_0', v_0', ρ_0') is a small perturbation.
We assume that at time t, the solution of our model (1) has the structure

$$(u, v, \rho) = (u^e, v^e, \rho^e) + \left(u', v', \rho'\right).$$

Let us introduce the new variables $\theta = \dfrac{\partial \rho}{\partial z}$, $\alpha = \dfrac{\partial u}{\partial z}$ and $\beta = \dfrac{\partial v}{\partial z}$. The Richardson number, in terms of these variables, is

$$R = -\frac{g}{\rho_0} \frac{\theta}{(\alpha^2 + \beta^2)} = R\left(\alpha, \beta, \theta\right),$$

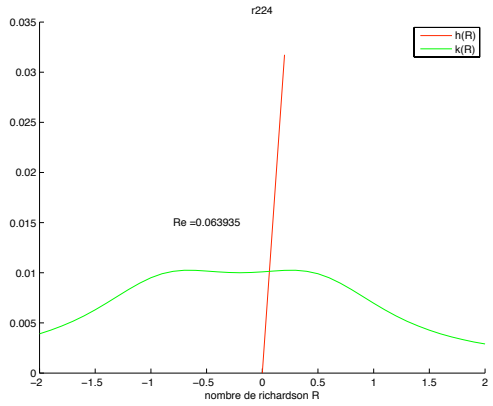

Figure 2:
Solution of the equation for equilibrium Richardson numbers for new model.

and consequently the turbulent diffusions are functions of (α, β, θ). Then, the equations satisfied by the perturbation are

$$\begin{cases} \dfrac{\partial u'}{\partial t} - \dfrac{\partial}{\partial z}\left(f_1\left(\alpha,\beta,\theta\right)\ \left(\alpha^e+\alpha'\right)\right) = 0, \\ \dfrac{\partial v'}{\partial t} - \dfrac{\partial}{\partial z}\left(f_1\left(\alpha,\beta,\theta\right)\ \left(\beta^e+\beta'\right)\right) = 0, \\ \dfrac{\partial \rho'}{\partial t} - \dfrac{\partial}{\partial z}\left(f_2\left(\alpha,\beta,\theta\right)\ \left(\theta^e+\theta'\right)\right) = 0. \end{cases} \tag{29}$$

Set $\mathcal{F} = f_1\left(\alpha,\beta,\theta\right) - f_1\left(\alpha^e,\beta^e,\theta^e\right)$ and $\mathcal{G} = f_2\left(\alpha,\beta,\theta\right) - f_2\left(\alpha^e,\beta^e,\theta^e\right)$. Taylor expansion yields

$$\mathcal{F} = \left(\alpha-\alpha^e\right)\ \frac{\partial f_1}{\partial \alpha}\ \left(\alpha^e,\beta^e,\theta^e\right) + \left(\beta-\beta^e\right)\ \frac{\partial f_1}{\partial \beta}\ \left(\alpha^e,\beta^e,\theta^e\right) + \left(\theta-\theta^e\right)\ \frac{\partial f_1}{\partial \theta}\ \left(\alpha^e,\beta^e,\theta^e\right) + \cdots \tag{30}$$

and

$$\mathcal{G} = \left(\alpha-\alpha^e\right)\ \frac{\partial f_2}{\partial \alpha}\ \left(\alpha^e,\beta^e,\theta^e\right) + \left(\beta-\beta^e\right)\ \frac{\partial f_2}{\partial \beta}\ \left(\alpha^e,\beta^e,\theta^e\right) + \left(\theta-\theta^e\right)\ \frac{\partial f_2}{\partial \theta}\ \left(\alpha^e,\beta^e,\theta^e\right) + \cdots \tag{31}$$

Let us denote, for $k = 1, 2:\ f_k^e = f_k\left(\alpha^e,\beta^e,\theta^e\right)$,

$$\left(\frac{\partial f_k}{\partial \alpha}\right)^e = \frac{\partial f_k}{\partial \alpha}\left(\alpha^e,\beta^e,\theta^e\right),\ \left(\frac{\partial f_k}{\partial \beta}\right)^e = \frac{\partial f_k}{\partial \beta}\left(\alpha^e,\beta^e,\theta^e\right),\ \left(\frac{\partial f_k}{\partial \theta}\right)^e = \frac{\partial f_k}{\partial \theta}\left(\alpha^e,\beta^e,\theta^e\right).$$

We next replace f_1 and f_2 by their Taylor expansions (Equations (30) and (31)) in the equation satisfied by the perturbation (29), and neglect the second order terms. This yields a linear system of the form

$$\frac{\partial V}{\partial t} - A\frac{\partial^2 V}{\partial z^2} = 0, \tag{32}$$

where

$$A = \begin{pmatrix} f_1^e + \alpha^e \left(\frac{\partial f_1}{\partial \alpha}\right)^e & \alpha^e \left(\frac{\partial f_1}{\partial \beta}\right)^e & \alpha^e \left(\frac{\partial f_1}{\partial \theta}\right)^e \\ \beta^e \left(\frac{\partial f_1}{\partial \alpha}\right)^e & f_1^e + \beta^e \left(\frac{\partial f_1}{\partial \beta}\right)^e & \beta^e \left(\frac{\partial f_1}{\partial \theta}\right)^e \\ \theta^e \left(\frac{\partial f_2}{\partial \alpha}\right)^e & \theta^e \left(\frac{\partial f_2}{\partial \beta}\right)^e & f_2^e + \theta^e \left(\frac{\partial f_2}{\partial \theta}\right)^e \end{pmatrix}, \quad V = \begin{pmatrix} u' \\ v' \\ \rho' \end{pmatrix},$$

Linear stability will follow if all eigenvalues λ_k of A, $k = 1, 2, 3$ have positive real parts. Indeed, this will ensure that the initial perturbation in the linearized system is totally damped as $t \to +\infty$ and its solution will converge to the steady solution.
To verify that all the λ_k have positive real parts, it is enough to prove that three independent invariants of matrix A are positive. A lengthy calculation yields

$$Trace(A) = 2f_1(R) + f_2(R) + R(f_2'(R) - 2f_1'(R));$$
$$Det(A) = f_1(R)(f_1(R)f_2(R) + Rf_1(R)f_2'(R) - 2Rf_2(R)f_1'(R));$$
$$Trace(AdjA) = 2f_1(R)f_2(R) + 2f_1(R)Rf_2'(R) - 2f_2(R)Rf_1'(R) + f_1(R)^2 - 2f_1(R)Rf_1'(R).$$

Some algebra shows that all of them are strictly positive for the three models we are considering, when $R \geq 0$. Thus, we conclude that all these models are linearly stable for $R \geq 0$.
Also, for each model we also obtain a range of negative Richardson numbers, for which it is linearly stable. This is a rather surprising result, as these ranges correspond to physically unstable configurations.

6 Numerical discretization

We have analyzed the stability of a standard conservative semi-implicit discretization of the PDEs appearing in model (1). We discretize initially by piecewise affine finite elements. This next yields a conservative finite difference discretization by using quadrature formulae to approximate the non-linear integrals. This is the kind of discretization used in practice by physical oceanographers.
To describe it, assume that the interval $[-h, 0]$ is divided into N subintervals of length $\Delta z = h/(N-1)$, with nodes $z_i = -(i-1)\,h\,\Delta z$, $i = 1, \cdots, N-1$, and construct the finite element space

$$V_h = \{ w_h \in C^0([-h, 0]) \,|\, w_{h|]z_{i-1}, z_i[} \text{ is affine}, i = 1, \cdots, N;\ w_h(-h) = 0 \}. \tag{33}$$

The equation for u, for instance, assuming $u_b = 0$ for simplicity, is discretized by linearization of f_1 as

$$\text{Obtain} \quad u_h \in V_h \quad \text{such that}$$

$$(P_h) \quad \int_{-h}^{0} \frac{u_h^{n+1}-u_h^n}{\Delta t}\, w_h + \int_{-h}^{0} f_1(R_h^n)\, \partial_z u_h^{n+1} \partial_z w_h = L^{n+1}(w_h), \quad \forall w_h \in V_h, \tag{34}$$

where $L^{n+1}(w_h) = V_1^{n+1}\, w_h(0)$. The case $u_b \neq 0$ also fits this discretization up to a standard change of L^{n+1}.

This discretization is stable under the hypothesis that the turbulent viscosity f_1 is uniformly bounded and positive:

$$\text{There exist} \quad 0 < \nu \leq M \quad \text{such that} \quad \nu \leq f_1(R) \leq M, \quad \forall R \in \mathbb{R}. \tag{35}$$

Let us denote by u_h the continuous piecewise affine function from $[0,T]$ on to V_h whose value in t_n is u_h^n, and by L_h the piecewise constant in time whose value in $]t_n, t_{n+1}[$ is L^{n+1}. This function is defined a. e. in $[0,T]$. Both u_h and L_h also depend on Δt, but we prefer this notation for simplicity as it is not confusing.

For simplicity of notation, we shall denote $L^p(L^q)$ the space $L^p((-h,0); L^q(0,T))$ and similarly the spaces $L^p(H^k)$. Our stability result is the following

Lemma 6.1 *Under hypothesis (35), there exists a constant $C > 0$ such that*

$$\|u_h\|_{L^\infty(L^2)} + \|u_h\|_{L^2(H^1)} + \|\partial_t u_h\|_{L^2(H^{-1})} \leq C\, \|L\|_{L^2(H^{-1})}.$$

Note that $\|L\|^2_{L^2(H^{-1})} \leq C' \sum_{n=1}^{N} \Delta t\, |V_1^{n+1}|^2$.

Proof of Lemma 6.1 The estimates for u_h in $L^\infty(L^2)$ and in $L^2(H^1)$ are standard, by taking $w_h = u_h^{n+1}$ and using the identity

$$(a-b)a = \frac{1}{2}|a|^2 - \frac{1}{2}|b|^2 + \frac{1}{2}|a-b|^2, \quad \text{for} \quad a, b \in \mathbb{R}.$$

The estimate for $\partial_t u_h$ is more involved, because as f_1 is not constant, the usual techniques to obtain estimates in $L^2(L^2)$ fail. However, we may obtain estimates in $L^2(H^{-1})$ as follows: Let Π_h denote the orthogonal projection from $L^2(-h,0)$ on to V_h. As V_h is a 1D finite element space with fixed element size, Π_h is also stable in $H^1(-h,0)$ (Cf. [5], Section 6): There exists a constant C_1 such that

$$\|\Pi_h w\|_{H^1(-h,0)} \leq C_1\, \|w\|_{H^1(-h,0)}, \quad \forall w \in H^1(-h,0). \tag{36}$$

Then, for any $w \in H^1(-h,0)$, and $t \in]t_n, t_{n+1}[$,

$$\begin{aligned} \int_{-h}^{0} \partial_t u_h(t)\, w &= \int_{-h}^{0} \frac{u_h^{n+1}-u_h^n}{\Delta t}\, \Pi_h w = -\int_{-h}^{0} f_1(R_h^n)\, \partial_z u_h^{n+1} \partial_z \Pi_h w + L^{n+1}(\Pi_h w) \\ &\leq \left(\|L^{n+1}\|_{H^{-1}(-h,0)} + M\, \|u_h^{n+1}\|_{H^1(-h,0)}\right) \|\Pi_h w\|_{H^1(-h,0)} \\ &\leq C_1 \left(\|L^{n+1}\|_{H^{-1}(-h,0)} + M\, \|u_h^{n+1}\|_{H^1(-h,0)}\right) \|w\|_{H^1(-h,0)}. \end{aligned} \tag{37}$$

Then,

$$\|\partial_t u_h(t)\|_{H^1(-h,0)} \leq C_1 \left(\|L^{n+1}\|_{H^{-1}(-h,0)} + M\, \|u_h^{n+1}\|_{H^1(-h,0)}\right)$$

and we conclude

$$\|\partial_t u_h\|_{L^2(H^{-1})} \leq C_2 \left(\|u_h\|_{L^2(H^1)} + \|L\|_{L^2(H^{-1})} \right).$$

•

To obtain a finite-difference discretization, we approximate the integral of the non-linear term appearing in (P_h) by the mid-point rule. Denote by φ_i the canonical piecewise affine basis function of V_h associated to node z_i; i. e., $\varphi_i(z_j) = \delta ij$. This quadrature formula yields, for $i = 2, \cdots, N$,

$$\int_{-h}^{0} f_1(R_h^n)\, \partial_z u_h^{n+1} \partial_z \varphi_i \simeq f_1(R_{i-1/2}^n) \frac{u_i^{n+1} - u_{i-1}^{n+1}}{\Delta z} + f_1(R_{i+1/2}^n) \frac{u_i^{n+1} - u_{i+1}^{n+1}}{\Delta z} \tag{38}$$

where

$$R_{i-1/2}^n = -\frac{g}{\rho_{ref}} \frac{(\rho_i^n - \rho_{i-1}^n)/\Delta z}{\left[|u_i^n - u_{i-1}^n|^2 + |v_i^n - v_{i-1}^n|^2 \right] / (\Delta z)^2},$$

Now, applying mass-lumping to the mass integral appearing in (P_h) when $w_h = \varphi_i$, we obtain the finite-difference scheme

$$\frac{u_i^{n+1} - u_i^n}{\Delta t} - \frac{f_1(R_{i-1/2}^n) u_{i-1}^{n+1} - \left[f_1(R_{i-1/2}^n) + f_1(R_{i+1/2}^n) \right] u_i^{n+1} + f_1(R_{i+1/2}^n) u_{i+1}^{n+1}}{(\Delta z)^2} = 0, \tag{39}$$

For $i = N$, the same procedure yields

$$\frac{u_N^{n+1} - u_N^n}{\Delta t} + f_1(R_{N-1/2}^n) \frac{u_N^{n+1} - u_{N-1}^{n+1}}{\Delta z} = V_1^{n+1} \tag{40}$$

To take into account the discretizations used in practice, we have replaced this equation by a more standard finite difference discretization of the Neumann condition,

$$f_1(R_{N-1/2}^n) \frac{u_N^{n+1} - u_{N-1}^{n+1}}{\Delta z} = V_1^{n+1} \tag{41}$$

This equation allows to compute u_N^{n+1} from u_{N-1}^{n+1}. So we may construct our discretization in terms of the unknowns $U^{n+1} = (u_2^{n+1}, \cdots, u_{N-1}^{n+1})$ and similarly for v and ρ. In matrix form, this discretization reads

$$A^{n+1}\, U^{n+1} = B^{n+1},$$

where A^{n+1} and B^{n+1} respectively are the tridiagonal matrix and the vector array defined with obvious notation by

$$A_{i-1,i}^{n+1} = -\alpha_{i-1/2}^n,\ A_{i,i}^{n+1} = 1 + \alpha_{i-1/2}^n + \alpha_{i+1/2}^n,\ A_{i+1,i}^{n+1} = -\alpha_{i+1/2}^n, \quad i = 2, \cdots, N-2;$$

$$A_{N-2,N-1}^{n+1} = -\alpha_{N-3/2}^n, \quad A_{N-1,N-1}^{n+1} = 1 + \alpha_{N-3/2}^n;$$

$$B^{n+1} = (u_2^n + \alpha_{3/2}^n\, u_b^n, u_3^n, \cdots, u_i^n, \cdots, u_{N-2}^n, u_{N-1}^n + \frac{\Delta t}{\Delta z}\, V_1)^t,$$

where

$$\alpha_{i-1/2}^n = \frac{\Delta t}{(\Delta z)^2}\, f_1(R_{i-1/2}^n),$$

and we have included a possibly non-zero Dirichlet boundary condition at $z = -h$: $u_1^n = u_b^n$. This discretization verifies a maximum principle:

Lemma 6.2 *If the initial data, u_b^n and V_1 are positive, then u_h is positive in $[-h, 0] \times [0, T]$.*

Proof. As $f_1 \geq 0$, then A^{n+1} is an M-matrix: It is irreducible, diagonal dominant, strictly for the first line, and all non-diagonal entries are non-positive. Then $(A^{n+1})^{-1}$ has positive entries, and consequently all the u_i^n are positive. •

7 Numerical tests

To test the performances of our new model, we have simulated two realistic flows, and we have compared the results of the new model with those of PP and Gent models. These flows correspond to the Equatorial Pacific region called the West-Pacific Warm Pool, located at the equator between $120°E$ and $180°E$. In this region the sea temperature is high and almost constant along the year $(28 - 30°C)$. The precipitations are intense and hence the salinity is low.

We have also tested the non-linear stability of steady solutions. In all three tests, we have been able to obtain grid-independent results, in the sense that they remain practically unchanged when Δz and Δt decrease.

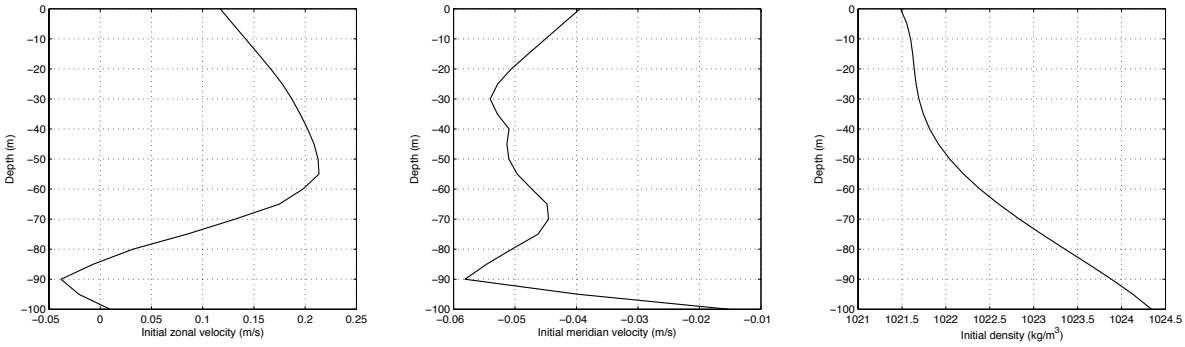

Figure 3: Initial zonal velocity, meridian velocity and density profiles (from left to right).

7.1 Mixed layer induced by wind stress

We initialize the code with data from the TAO (Tropical Atmosphere Ocean) array (McPhaden [9]), which have been used in many numerical simulations.

Here, we present the results corresponding to a mixed layer induced by the wind stress, using initial velocity and density profiles measured at $0°N, 165°E$ for the time period between the 15th June 1991 and the 15th July 1991, displayed in Figure 3. Observe that the initial density profile does not present a mixed layer.

We used the numerical discretization of model (1) described in section 6. The buoyancy flux is $-1.10^{-6}\ kg.m^{-2}.s^{-1}$ $(\simeq -11\ W/m^2)$, which is realistic for this region. Indeed, Gent reports in [3] that the heat flux is in the range $[0\,W/m^2, 20\,W/m^2]$ between $140°\ E - 180°\ E$ and $10°\ S - 10°\ N$.

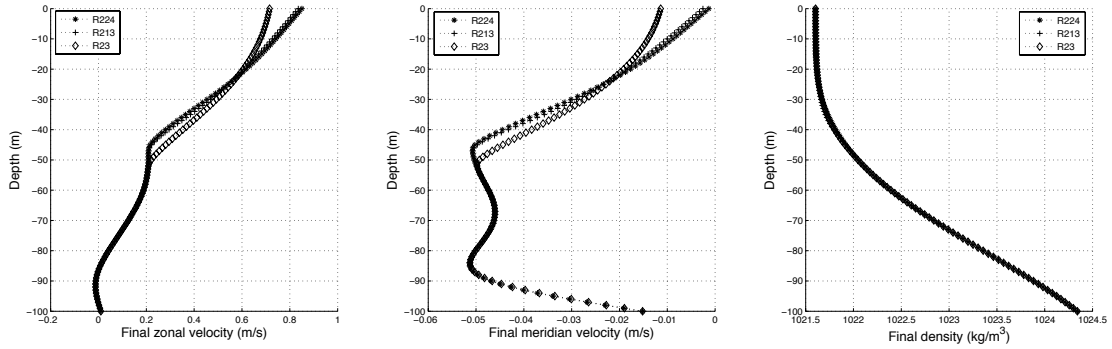

Figure 4: Comparison of three turbulence models: R213 (PP), R23 (Gent), R224 (new one). Full mixing layer.

We have taken as boundary conditions, a *zonal wind* (u_1) equal to 8.1 m/s (eastward wind) and a *meridional wind* (u_2) equal to 2.1 m/s (northward wind). These values are larger than the measured ones, to force the formation of a mixed layer. Figures 4 and 5 display the results

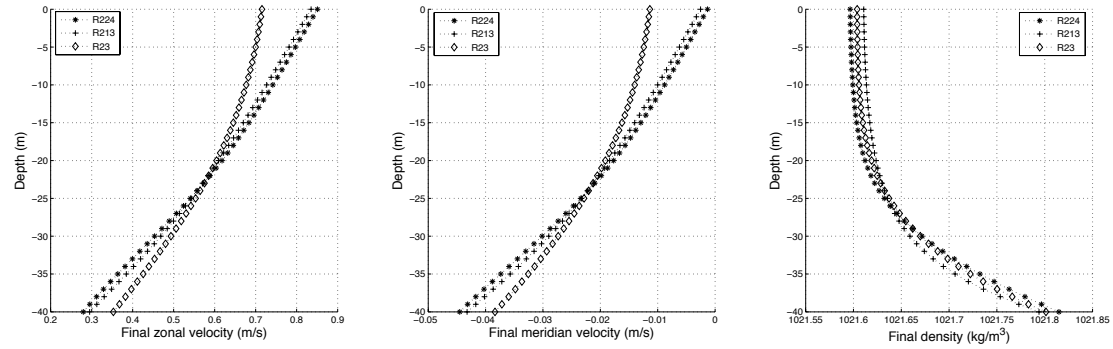

Figure 5: Comparison of three turbulence models: R213 (PP), R23 (Gent), R224 (new one). Upper 40m of mixing layer.

corresponding to $t = 48$ hours with $\Delta z = 1m$ and $\Delta t = 60s$. On figure 4 we represent the whole mixing layer, and in figure 5, the upper 40m of this layer. The plots for density profiles show the formation of a mixed layer of some 20m depth, corresponding to almost constant density values. A pycnocline (strong gradient below a zone where the density is almost constant) is formed below the mixed layer. This is a characteristic density profile for a well-mixed turbulent surface layer. It is striking that the density profiles simulated by the three models are quite similar. Velocity and density profiles are quite close for PP and the new model, while the velocity provided by Gent model is somewhat different, mainly near the surface.
From this result we may accept the physical validity of our new model, as it yields results very close to those of the standard PP model.

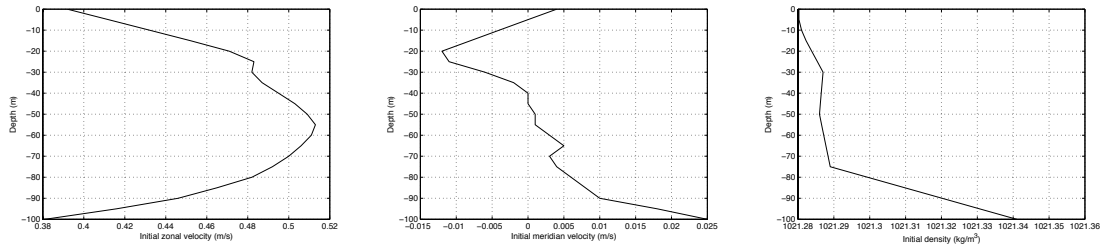

Figure 6: The initial profiles for zonal velocity, meridian velocity and density (from left to right).

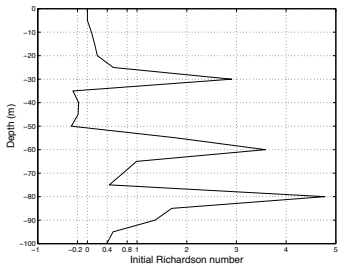

Figure 7: Initial Richardson numbers, corresponding to the initial profiles of figure 6.

7.2 A static instability zone in the initial density profile

In this test we initialize the code with the 17th November 1991 data. The initial profiles are displayed on figure 6. We observe a seventy meters deep mixed layer, which is not homogeneous in the sense that it is not well mixed. Furthermore, the initial density profile displays a static instability zone between $-30\,m$ and $-50\,m$. This is not an isolated situation, as there TAO data show similar instability zones for several days between the 16th and the 22th November 1991.
As we may observe in figure 7.2, the initial Richardson number R^0, is negative in the depth range $[-50m, -30m]$, taking values smaller than $R^0 = -0.2$ at $z = -45\,m$. The PP and Gent models yield negative turbulent diffusions for these data, and can not be run. In its turn, our new model has positive diffusivity for all values of the Richardson number.
The new model is integrated for 48 hours. We present the results corresponding to $\Delta z = 5\,m$, and $\Delta t = 60s$, with boundary conditions $u_1 = 11.7\,m.s^{-1}$ (eastward wind), $u_2 = 0.4\,m.s^{-1}$ (northward wind) and buoyancy flux $Q = -1.10^{-6}\,kg.m^{-2}.s^{-1}$ ($\simeq -11W/m^2$).
The results are displayed on figure 8. Our model produces a homogeneous seventy meters deep mixed layer, with a structure quite similar to test Case 1, where the initial density presented a stable configuration. The density remains almost constant down to $z \simeq -70$, and presents a pycnocline immediately below. The profiles for velocities are quite smooth, as correspond to a well-mixed layer.

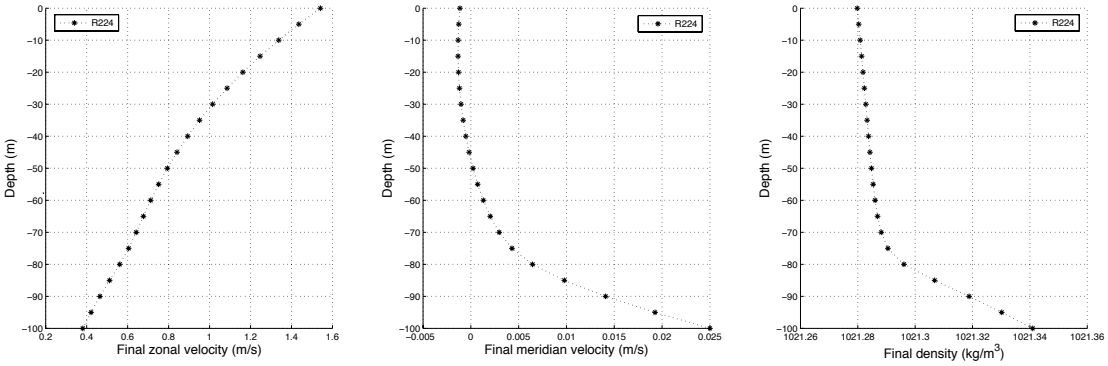

Figure 8: Profiles for zonal velocity, meridian velocity and density (from left to right) computed with the new model.

7.3 Case 3: Analysis of non-linear stability of equilibrium solutions

In section 4 we proved that equilibrium solutions are linearly stable for our three models. Here we investigate by numerical simulation wether these equilibria also are non-linearly stable, using real data as initial conditions. Our results also show a non-linear stability of all equilibria solutions, that act in fact as point-wise attractors whenever we apply a negative buoyancy flux at the surface.

The initial profiles represent the ocean mean state on June 17, 1991 (figure 9). We have used the following boundary conditions : buoyancy flux $Q = -1.10^{-6}\, kg.m^{-2}.s^{-1}$ ($\simeq -11\, W/m^2$), $u_b = 5.4\, m.s^{-1}$ (eastward wind) and $v_b = 0.9\, m.s^{-1}$ (northward wind).

We have chosen this initial data as the density profile presents a thirty five meters deep mixed layer, and we want to analyze wether this mixed layer evolves to a non-constant density.

We have run the three models for 10.000 hours (about 13 months and a half). The numerical results are displayed in figure 10. The three turbulence models give linear profiles for the simulated time, with slopes of the same sign. We observe that the velocity for PP and the new model are rather close, while the discrepancy in density is larger. The Gent model presents a larger discrepancy in velocities.

We have observed that the convergence of all models to steady states takes times of the order of several months. This time scale is much larger than that needed to generate a typical homogeneous mixed layer, which is of the order of a few days (in all cases with steady boundary data). This may explain why these linear profiles for the mixing layer are not found in real surface layers, as the boundary data usually change in time scales of the order of hours. Even the formation of a homogeneous mixed layer is not possible if these data change too fast.

Finally, to check that we compute the right steady states, we compare in figure 11 the solution computed at $t = 10.000$ hours and the theoretical steady state (25), (26), (27), for the new model, corresponding to $R^e = 0.0639$ (See figure 2). We observe that both are very close.

Several tests with all three models, using different initial data yield qualitative and quantitative similar results. We conclude that the equilibria states are non-linearly stable for negative heat

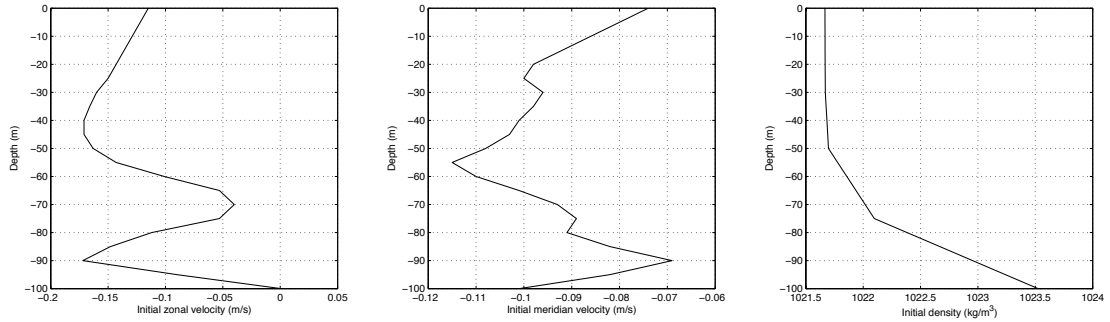

Figure 9: Profiles for zonal velocity, meridian velocity and density (from left to right) to test the non-linear stability of all three models.

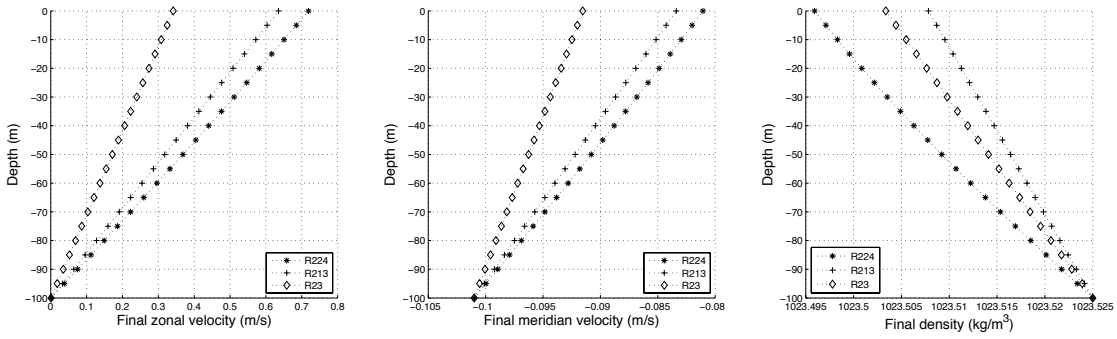

Figure 10: Profiles for zonal velocity, meridian velocity and density (from left to right) for all three models, computed at $t = 10.000$ hours.

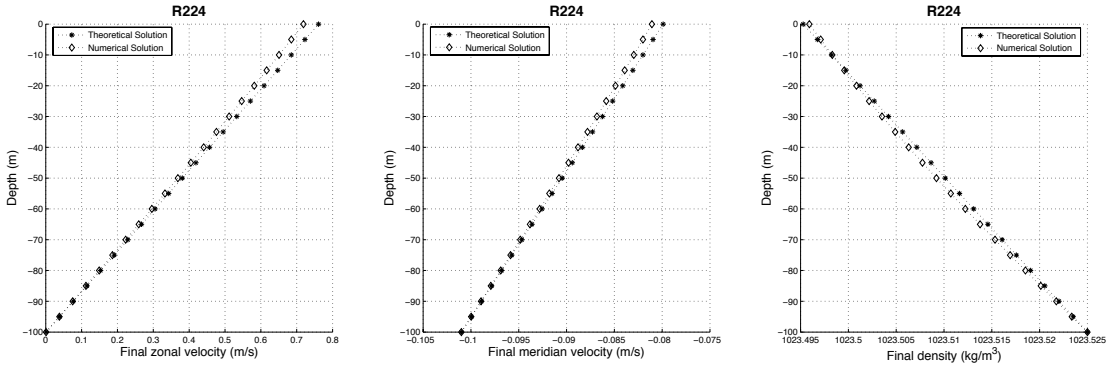

Figure 11: Comparison of solution computed at $t = 10.000$ hours versus theoretical steady states, for new model (R224).

fluxes. Even more, that these equilibria behave as point attractors with associated time scales of the order of the year.

8 Conclusions

In this paper we have analyzed from the mathematical point of view several aspects of algebraic turbulence models for oceanic turbulent mixing layers. This analysis has partially confirmed that these models are well suited as mathematical models. Specifically, we have proved that the usual conservative finite difference schemes used to solve them are stable, at least in a week sense. We have also proved that these schemes have equilibria states which are linearly stable, and appear numerically to be non-linearly stable.

Also, we have been able to analyze the well-possedness of a simplified model. The general case remains an open problem, due to the lack of estimates for the gradients of velocity and density in a sense strong enough. This seems a rather hard mathematical problem. However, numerically all the considered cases show a formal convergence to some solution, in the sense that we obtain grid and time step-independent numerical solutions.

Acknowledgements

Research of T. Chacón and M. Gómez partially funded by Spanish DIG grant MTM2006-01275.

References

[1] B. Blanke and P. Delecluse, *Variability of the tropical atlantic ocean simulated by a general circulation model with two different mixed-layer physics*, J. Phys. Oceanography, 23 (1993), pp. 1363–1388.

[2] P. Gaspar, Y. Gregoris, and L. J. M., *A simple eddy kinetic energy model for simulations of the oceanic vertical mixing: test at station papa and long-term upper ocean study site*, J. Geophys. Research, 16 (1990), pp. 179–193.

[3] P. R. Gent, *The heat budget of the toga-coare domain in an ocean model*, J. Geophys. Res., 96 (1991), pp. 3323–3330.

[4] H. Goosse, E. Deleersnijder, T. Fichefet, and M. H. England, *Sensitivity of a global coupled ocean-sea ice model to the parametrization of vertical mixing*, J. Geophys. Res., 104 (1999), pp. 13681–13695.

[5] J. E. P. J. H. Bramble and O. Steinbach., *On the stability of the l^2 projection in h^1.*, Math. Comp., 7 (2001), pp. 147–156.

[6] W. G. Large, C. McWilliams, and S. C. Doney, *Oceanic vertical mixing : a review and a model with a nonlocal boundary layer parametrization*, Rev. Geophys., 32 (1994), pp. 363–403.

[7] J. L. Lions, *Quelques méthodes de résolution de problèmes aux limites non linéaires*, Dunod, Paris, 1969.

[8] G. Madec, P. Delecluse, M. Imbard, and C. Levy, *O.p.a. version 8.0. ocean general circulation model, reference manual*, 1997. Technical report.

[9] M. McPhaden, *The tropical atmosphere ocean (tao) array is completed*, Bull. Am. Meteorol. Soc, 76 (1995), pp. 739–741.

[10] G. Mellor and T. Yamada, *Development of a turbulence closure model for geophysical fluid problems*, Reviews of Geophysics and Space Physics, 20 (1982), pp. 851–875.

[11] R. C. Pacanowski and S. G. H. Philander, *Parametrization of vertical mixing in numericals models of the tropical oceans*, J. Phys. Oceanogr., 11 (1981), pp. 1443–1451.